PERGAMON

Journal of Structural Geology 22 (2000) 307–322

JOURNAL OF STRUCTURAL GEOLOGY

www.elsevier.nl/locate/jstrugeo

Scaling properties of normal fault populations in the western Corinth Graben, Greece: implications for fault growth in large strain settings

G. Poulimenos*

Department of Geology, General-Marine Geology and Geodynamics Division, University of Patras, Patras, Greece

Received 12 May 1999; accepted 22 September 1999

Abstract

A variety of one-dimensional and two-dimensional map techniques of fractal analysis have been employed to investigate the scaling properties of the dominant WNW-trending normal fault population of the western Corinth graben in central Greece. To assess possible constraints on fault geometry during fault growth, the data have been compiled separately from the northern and southern domains of the graben, which have experienced differing amounts of finite strain. Based on power-law distributions of the fault throw, the applied extension is estimated at 30% and 22% for the northern and southern domains, respectively. However, the fault spacing and fault length populations in both domains obey similar power-law relationships. These conclusions are also supported by maximum throw vs. trace-length data, which demonstrate that the faults in the northern domain have systematically higher values for the slip-to-length ratios than those in the southern domain. It is proposed that the Corinth graben has reached 'fracture saturation' that is, the fault spacing stops evolving and displacement increases rather than faults lengthening to accommodate the increasing extension. This growth process, consistent with throw distributions along individual faults, may be explained either in terms of a stress feedback mechanism, or by the mechanical interaction between the WNW-trending normal faults with a set of NNE-trending transverse faults.

1. Introduction

Over the past decade, there has been considerable research into quantitative characterization of fault populations for the purpose of gaining a better understanding of the processes governing the growth of faults. A general result of this research is that a wide variety of fault population attributes, such as trace-length, spacing and displacement (e.g. Scholz and Cowie, 1990; Sornette, 1990; Walsh and Watterson, 1992; Peacock and Sanderson, 1994), can be described in many cases by simple power-laws. These power-law, or 'fractal', relationships are defined as:

$$N = Cr^{-D} \tag{1}$$

where N is the numerical rank of each fault in a list ordered by the fault parameter magnitude (r), D is the fractal dimension and C is a constant of proportionality. For fault populations that follow fractal scaling laws, a plot of $\log N$ vs. $\log r$ will define a straight line with slope of $-D$ and with an intercept on the ordinate equal to $\log C$. High values of D imply a higher proportion of small objects than large objects in the population. However, due to the inherent complexities of faulting there is no general agreement on the scaling relationships between different fault parameters. This most probably relates to the large scatter in maximum displacement (d) against trace length (l) data in most fault data sets (Cowie and Scholz, 1992b; Gillespie et al., 1992), so different conceptual fault growth models have been invoked. According to one concept, a fault is a single smooth continuous surface of displacement, which becomes larger as the slip across it increases (Watterson, 1986; Walsh and Watterson, 1987, 1988;

* Correspondence address: P.O. Box 67269, 151 02 Melissia, Athens, Greece.

E-mail address: geopoul@ars.net.gr (G. Poulimenos).

0191-8141/00/$ - see front matter
PII: S0191-8141(99)00152-2

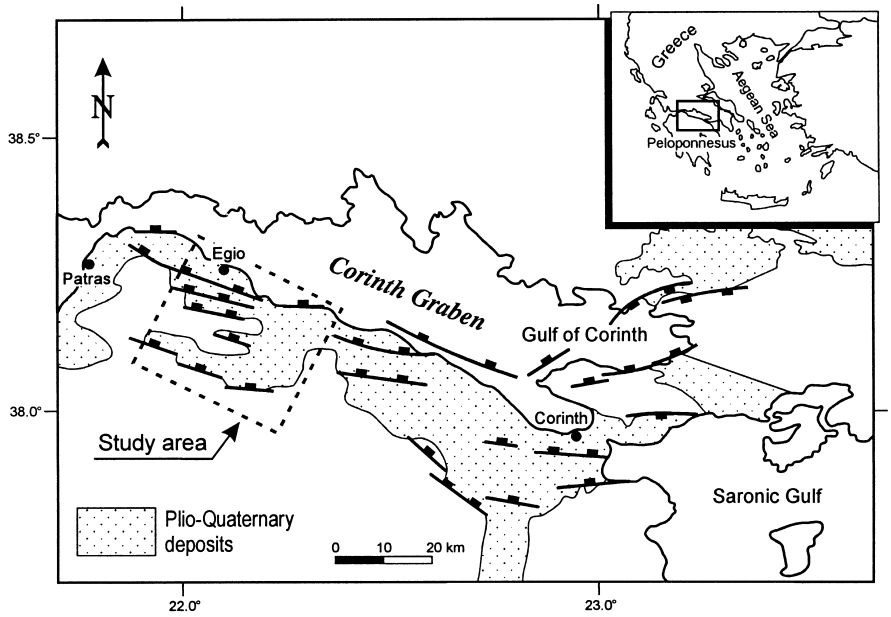

Fig. 1. Simplified geological map of the Corinth graben showing approximate boundaries of the study area. The inset map illustrates the location of the Corinth Graben relative to mainland Greece.

Marrett and Allmedinger, 1991; Cowie and Scholz, 1992a, b; Gillespie et al., 1992). According to a second concept, faults grow primarily by the linkage of precursor segments, which cannibalize small faults to create larger faults (Segall and Pollard, 1980; Ellis and Dunlap, 1988; Martel et al., 1988; Peacock and Sanderson, 1991; Cartwright et al., 1995). Further consideration of fault systematics allows different scaling laws to be applied over specific ranges of fault size (Scholz and Aviles, 1986; Turcotte, 1989; Cowie and Scholz, 1992c), as well as between successive stages of fault growth (Main, 1988; Filbrandt et al., 1994; Cartwright et al., 1995; Cladouhos and Marrett, 1996). Even with these uncertainties, there is ample documentation to suggest that as fault displacement accumulates, faults grow in size, i.e. their surface area and length increase.

Despite the large amount of theoretical and experimental work and natural data sets, which support these types of growth models, opposing opinions exist. Experimental data show that when the applied strain reaches a certain value, the fracture spacing remains nearly constant, and increasing deformation is accommodated by further opening of the existing fractures, rather than continued fracture propagation (Wu and Pollard, 1992, 1995). A body of rock that is at such a stage of deformation is said to have reached 'fracture saturation'. Although this concept has long been discussed in the context of subsurface joint densities in oilfields (Narr, 1991), its applicability to natural fault populations has only recently been suggested (Brooks et al., 1996; Cowie, 1998).

This paper attempts to test the applicability of the proposed fault growth processes in the active basins of the Aegean region, one of the most rapidly extending continental areas in the world. For this purpose, a number of different fault parameters from the western Corinth Graben of central Greece have been measured and analyzed. Domains of differing amounts of fault strain have been identified, and thus the Corinth Graben offers an excellent opportunity to study changes in fault geometry during progressive deformation. This study starts with a brief overview of the regional structure and geological history of the Corinth Graben to provide a background to the analyses of the displacement, length and spatial distributions of the fault populations. The population data are then modeled addressing implications for fault growth in this area. Finally, possible physical explanations for the proposed model are discussed.

2. Geological background

It is well known that continental Greece has been an area of rapid N–S ($\pm 20^{\circ}$) crustal extension since early Pliocene times (e.g. McKenzie, 1978; Le Pichon and Angelier, 1981; Roberts, 1996a), or earlier (Jolivet et al., 1994). In the Gulf of Corinth, the recent high extensional strain rates have been accommodated by a series of seismically active NNE-dipping fault zones, which are responsible for the development of characteristic graben and asymmetric half graben basins (e.g. Roberts and Jackson, 1991; Poulimenos and Doutsos,

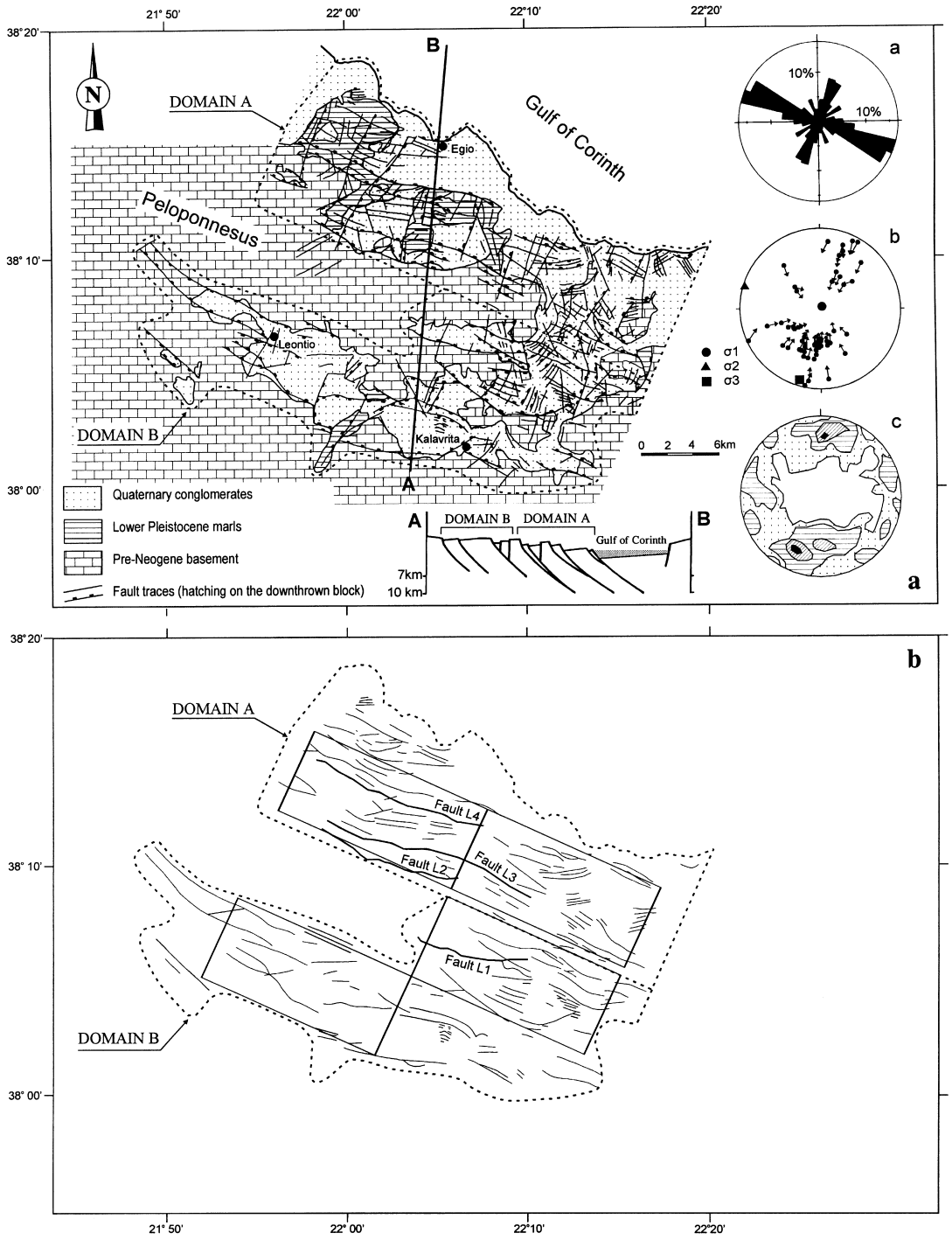

Fig. 2. (a) Geological map of the western Corinth graben showing the studied areas (stippled boundaries), and geometric and kinematic fault data. The rose diagram (a) for fault lengths demonstrates the WNW dominant fault trend. The slip linear plot (b) of kinematic indicators on fault planes determines a NNE-trending minimum compressional stress (σ_3). The stereoplot (c) of 350 faults shows a dominant dip of the outcrop-scale faults averaged at 70° (contours: 1–3–5–7%). The cross-section (AB) outlines the crustal deformation across the Corinth graben (modified from Doutsos and Poulimenos, 1992). (b) Fault map showing the WNW normal fault sets used in this study. Also shown are the faults included in the throw distribution analysis and the multi-box initial grids used for the box-counting run.

1997; Jackson and McKenzie, 1988; Ambraseys and Jackson, 1990) (Fig. 1).

The Corinth graben constitutes a 100-km-long and 40-km-wide structural province, which is superimposed on limestone dominated thrust with a N–S structural grain. The normal fault pattern consists of two major trends (Doutsos et al., 1988; Poulimenos et al., 1989) (Fig. 2a): (1) WNW-trending longitudinal normal faults; and (2) transverse faults with a predominantly NNE trend (Fig. 2a, plot a). Transverse faults show vertical displacements of up to 250 m and normal to oblique senses of movement with dips close to vertical, whereas the WNW-trending normal faults have dips between 50° and 90° and throws of up to 800 m (Fig. 2a, plot c). Both sets have been simultaneously active, producing a rectangular pattern, with differential subsidence during sedimentation (Poulimenos et al., 1993). The sedimentary fill, clearly controlled by an increase in subsidence through time, is organized into basin-wide packages, though syndepositional deformation patterns have been observed. Within these packages, upper Pliocene–lower Pleistocene marine to lacustrine marls are capped by conglomeratic terrestrial and marine/lacustrine fan-delta sequences of late Quaternary age (Doutsos and Piper, 1990).

In the western sector of the graben, tectono-sedimentary evidence and fault slip analysis delineate three major WNW-trending rifted domains of different amounts of deformation (Doutsos and Poulimenos, 1992; Fig. 2a, cross-section AB). The northernmost domain is occupied by the present day Gulf of Corinth and has experienced the highest regional extension. Extension is accommodated by a series of major active faults which run along its southern margin allowing marine conditions to be established throughout the region since the early Pleistocene (Brooks and Ferentinos, 1984). A 10-km-wide coastal zone of the northern Peloponnesus (Domain A) comprises the exposed end of the Pleistocene marine basin. WNW-trending faults that involve vertical displacements of up to 800 m produce $\approx$20% extension (Poulimenos, 1993). The southernmost domain, referred to herein as domain B, includes terrestrial intramontane basins of the Corinth graben which have developed during the late Quaternary. WNW-trending faults, that exhibit vertical displacements of up to 500 m, accommodate $\approx$10% extension (Poulimenos, 1993).

It is worth noting, however, that the extension estimates, based on cross-section balancing techniques along the cross-section AB (Fig. 2a), refer to the amount of extension accommodated by the map-scale faults within each domain. The stratigraphic record also supports the concept of differing amounts of extension experienced by the domains A and B. Thick fan-delta sequences, favored in settings of high tectonic activity (Boggs, 1987) have accumulated in the domain A, whereas braided river deposits, associated with lower tectonic activity settings have been involved in the filling of domain B. However, the extension is principally localized within the graben. This is mirrored in the basement areas, which are cut by degraded fault scarps that display no clear evidence of neotectonic activity.

3. The data sets

This paper examines displacement, spacing and trace-length scaling relationships for the onshore faults of the dominant WNW-striking normal fault set cutting into the western Corinth graben (Fig. 2b). Offshore faults have not been analyzed because the data uniformity is not as reliable as that on land. In order to investigate possible constraints on fault geometry and extension, so that the results might be used to develop a geometrical model for physical fault growth processes, the data analysis has been performed separately for the domains A and B of the graben (Fig. 2b).

The WNW-trending faults strike N80° to N130° (Fig. 2a, plot a). Kinematic indicators for this population suggest a minimum compressive stress (σ_3) oriented N20° (Fig. 2a, plot b). The computed tensor refers to an overall stress field in the western Corinth graben and may conflict with slip data along individual faults which suggest a slip direction ranging from NNW to NNE (Roberts, 1996a,b). Nevertheless, the WNW-trending faults develop sub-perpendicular to the extension direction and they are attributed to normal rifting produced by a purely extensional regime. The NNE-trending transverse faults are interpreted as either inherited 'passive' discontinuities that have been reactivated during extension, or as a result of variable displacement along normal faults. Movements along the transverse faults are essentially guided by the movements along the WNW-trending normal faults (cf. Colletta et al., 1988; Destro, 1995; Morewood and Roberts, 1997).

The fault parameters were obtained by analyzing geological cross-sections (one-dimensional techniques) and maps (two-dimensional techniques). One-dimensional sampling was performed along NNE-trending cross-sections at map and outcrop scales to assess the fault throw and spacing distributions. Faults are distinguished from joints only if they show displacement of a marker bed or brecciation. The sampling procedure involved random selection of cross-sections cutting into the graben fill, as well as the graben margins, and resulted in areas of varying fault density being measured. Faults in the basement areas, which are inactive or not active enough to dominate the geomorphology, are excluded from the analysis (see domain

boundaries in Fig. 2). In total, 40 cross-sections intersecting 330 faults were analyzed. Thus, the one-dimensional data are considered to be representative of the overall state of faulting in domains A and B. Throws on small faults exposed in road cuts were measured directly with a tape measure from the vertical offset of markers. These measurements ranged from an imposed resolution limit of 8 mm to $\approx$5 m with most of the values incorporating measurement errors of less than 2%. Measurements below the resolution limit were difficult to be made consistently in the weathered outcrops and therefore they were omitted. Throws on larger faults ($\geq$5 m) exposed in vertical cliffs up to 50 m height were measured by leveling techniques. Leveling probably resulted in errors of up to 5% for these measurements. Throws for map-scale faults in the range of 100–800 m were calculated by adding the maximum thickness of the sedimentary prism, which has been deposited on the hanging wall block of the fault, and the fault scarp height. The estimation of the maximum sediment thickness involved both the lower Pleistocene marls and the upper Quaternary conglomerates to provide maximum values for the total fault throw accumulated throughout Quaternary time. The major sources of uncertainty for these measurements are: a) the identification of the scarp crest on degraded hillslopes, b) the assumption that the topmost layers have not been eroded away, and c) the reliability of the stratigraphic correlations, which allow estimation for the total sediment thickness to be made. Therefore, it is felt that they incorporate uncertainties in the order of 10–15%. The spacing data, obtained from faults with throws above the imposed throw resolution limit of 8 mm, were gathered from road cuts, vertical cliffs and maps at scales of 1:5000–1:20,000 by measuring the lengths between successive intersections of faults in cross-section. The spacing measurements ranged from 0.2 m to 200 m for the outcrop-scale faults and from 50 m to 3000 m for the map-scale faults. Possible errors associated with these data are less than 10% and would be related to changes in dip and strike of the faults with respect to the trend of the sampling line.

There are several reasons for concentrating on one-dimensional data: First, dip-slip faults, even with throws less than several centimeters, can be accurately measured on vertical sections, which are readily available in this area and often of good quality. Secondly, the section data avoid some truncation and censoring problems associated with fault maps (Walsh et al., 1994; Pickering et al., 1995). Truncation (Heffer and Bevan, 1990), called Type-C censoring or left-hand truncation (Pickering et al., 1995), results from incomplete sampling of a population and causes the cumulative frequency distributions to fall off at small-scale values. Data within this 'fall off' are not representative of the distribution and should be excluded from the analysis (Pickering et al., 1995). Censoring (Jackson and Sanderson, 1992), called 'finite-range' effect or right-hand truncation (Pickering et al., 1995), refers to the underestimation of the large-scale values of a sample. Most fracture length statistics are affected by censoring as a number of fractures may extend beyond the boundary of the sampled area. This effect produces log-normal distributions at large-scale values which makes reliable estimation impossible, unless the data are corrected (Pickering et al., 1995).

However, most single cross-sections do not resolve a large enough number of faults to allow a reasonable estimate of the *D*-value. Therefore, multi-line data sets were utilized, derived from combined measurements along multiple transverses intersecting different faults. Such data sets, which do not contain repeated measurements from the same fault, can give consistent results close to the true distribution amongst the fault population (Pickering et al., 1996) and, therefore, have been widely used in fractal analysis (Walsh et al., 1991; Yielding et al., 1992; Westaway, 1994; Needham et al., 1996). From the linear transverses, the cumulative number of faults per meter was calculated, thereby normalizing the data and allowing comparison of displacement and spacing data from map to outcrop scale range. Combination of field and map data, however, implicitly assumes that: a) field sampling is representative of the fracturing in the basement and b) field and map data belongs to the same population (Jackson and Sanderson, 1992). Both assumptions seem valid for the Corinth graben. This is demonstrated by numerical analysis of combined map and field fault parameters which allowed estimation of the down-dip width of the graben-forming faults (Doutsos and Poulimenos, 1992) comparable to that determined by seismological studies (Rigo et al., 1996).

Two-dimensional data sets, focused on fault trace-length, were used to investigate, *d:l* relationships, the fault size–frequency distribution and the spatial clustering of faults as an additional approach to the one-dimensional spacing results. The two-dimensional data were obtained from maps at scale 1:20,000 which present interpretations of geologic and geomorphologic features, in terms of faults that have sustained offsets greater than 2 m through the Quaternary (Doutsos et al., 1988; Poulimenos, 1993; Fig. 2). Fault tips were accurately located by 1:5000 mapping, based on aerial photographs and field observations. Trace-lengths were determined for faults with lengths greater than 200 m by making tip-to-tip measurements. Fault scarps cross-cut by rivers and streams were considered to be the surface expression of a single fault. Trace-lengths shorter than 200 m were difficult to determine accurately, and thus, were not included here. It is worth considering the possible errors that are present in the

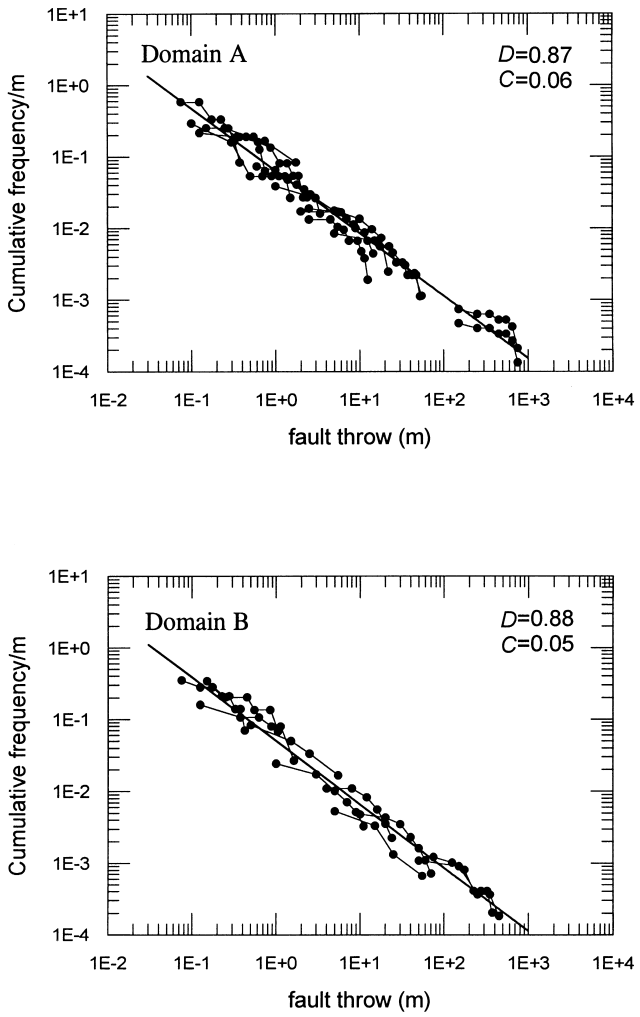

Fig. 3. Logarithmic cumulative frequency m^{-1} plots for multi-line, one-dimensional samples (lines) of fault throw from the domains A and B.

trace-length data. The fault throw resolution limit for which the fault map is considered complete was set to be about 2 m. This was done because it is difficult to resolve faults with throws of less than 2 m due to surficial modification by erosion processes. Thus, the fault tips are well located within 10–30 m and the trace-length measurements have errors that are probably no more than 5%. However, the fault-length population may be consistently underestimated because the fault tips are not points of zero throw but have throws of 2 m. The fault population covers an area of about 800 km^2 and consists of 170 individual fault traces, with lengths from 200 m to 18 km and with morphological offsets ranging from 2 m to 300 m. It is therefore suggested that it provides representative trace-length data suitable for fractal analysis.

4. Data analysis

4.1. Throw populations

The throw data from the domains A and B are plotted as multi-line population curves in log–log space in Fig. 3. The distribution plots consist of straight-line segments, which span at least four orders of magnitude and convincingly demonstrate power-law relationships. Least-squares fits to the data, ignoring deviations at the limits of the data sets, yield an overall D-value of 0.87 ± 0.02 for the domain A and 0.88 ± 0.02 for the domain B. The equivalent values of C are estimated at 0.06 ± 0.03 and 0.05 ± 0.03. These results suggest that the fault throws observed in the domains A and B belong to the same population.

Once the fault populations are scale invariant, then Eq. (2) provides a good approximation of the total throw on all faults with individual throw u (Scholz and Cowie, 1990):

$$\int_{u\min}^{u\max} DCu^{-D}\mathrm{d}u = \left[\frac{DC}{1-D}u^{1-D}\right]_{u\min}^{u\max} \quad (2)$$

The choice of $u_{\min}$ is somewhat arbitrary, however ≈ 1 mm is believed to be reasonable as this would represent the minimum size for a fault formed by the same physical process as larger faults (Walsh and Watterson, 1992; Pickering et al., 1996). Integration of Eq. (2) from 1 mm to the maximum observations (that is, 800 m for the domain A and 500 m for the domain B) gives values of cumulative throw per meter in the order of 0.84 and 0.61 for the domains A and B, respectively. Taking that the sampled faults dip at angles averaging 70° (Poulimenos et al., 1989; Fig. 2a, plot c), the corresponding fault heaves are estimated at 0.30 and 0.22, which correspond to extensional strains of 30% and 22% for the domains A and B, respectively. These estimates make the studied domains comparable with strain estimates obtained from other classic extensional terrains, such as the Paris Basin (Brunet and Le Pichon, 1982) and the Rhine graben (Richard and Groshong, 1996). Furthermore, they support the concept that the domain A has experienced a large amount of extension, which exceeds that of the domain B by a factor of ≈ 1.4. However, the inferred strains are much more than previously thought. This bias is not surprising and results from fault throw resolution effects in determination of total strain, as has been extensively discussed for fracture surveys (Scholz and Cowie, 1990; Walsh et al., 1991; Jackson and Sanderson, 1992). Indeed, integrating Eq. (2) over the throw resolution limit of 2 m imposed for the map-scale faults, we obtain extension estimates of 20% and 13.5% for the domains A and B, respectively, which fit well enough with those presented in the introduction

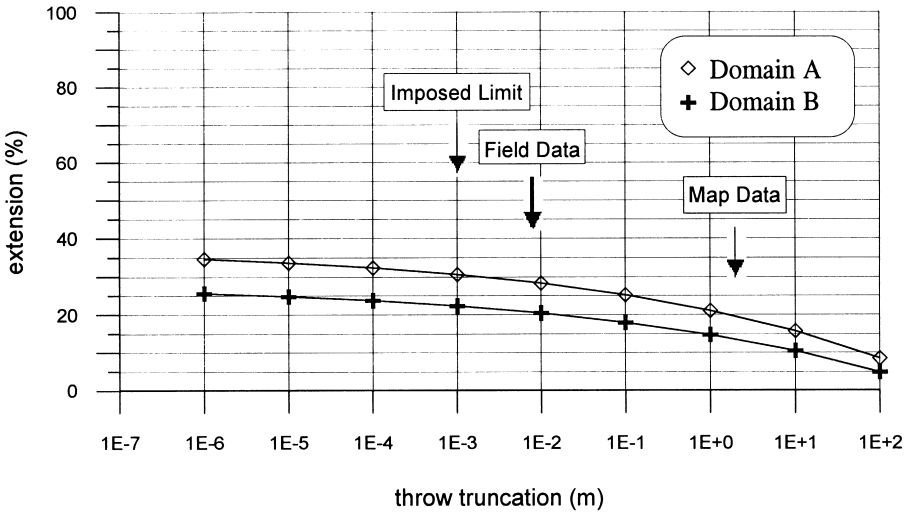

Fig. 4. Graph showing the calculated extension for the domains A and B against the truncation value of the fault throws entered in Eq. (2). The calculation is shown for the D and C values found in Fig. 3, fault dip averaged at 70°, and maximum fault throw of 800 m and 500 m for the domains A and B, respectively.

section of the paper (Poulimenos, 1993). The effects of other values of u_{min} on the extension estimates are shown on the graph of Fig. 4. Comparison of the extension values corresponding to the map and field data demonstrates that $\approx 10\%$ of the calculated extension for the domain A is taken up by the outcrop-scale faults and the remaining $\approx 2\%$ is accommodated on faults below the lower limit of field data resolution. The equivalent extension estimates for the domain B are 7% and 1.5%, respectively.

4.2. Spacing populations

The fault spacing data sets have been analyzed by the spacing population method (Harris et al., 1991). This method measures the distance between successive intersections of faults in cross-section, which are plotted on a normalized cumulative frequency plot.

The results for the domains A and B are shown in Fig. 5. The linear trends of the data that span over four orders of magnitude provide an indication of power-law relationships. Least-squares fits to the data, excluding the edge intervals of the data sets, yield for both of the studied areas power-law distributions of $D = 1.00 \pm 0.01$.

The fractal dimension provides a measure of the degree of clustering along a one-dimensional line sample. Lower D values indicate larger gaps and tighter clusters (Mandelbrot, 1983; Gillespie et al., 1993). The inferred D values therefore suggest a regular distribution of faults within and between the domains A and B. Thus, considering the extension estimates, it appears that the spacing distribution of the WNW-trending fault population stops evolving and remains constant as the extension proceeds.

4.3. Trace-length populations

The trace-length populations for the domains A and B are shown in Fig. 6(a and b). It is clear that the distribution plots have central straight portions that begin to curve as the data limits are approached. This overall convex upward appearance is interpreted as resulting from both left-hand truncation and finite-range effects which produce biased estimates of $D = 1.37 \pm 0.08$, $C = 82.04 \pm 12.15$ for domain A and $D = 1.37 \pm 0.10$, $C = 79.16 \pm 13.06$ for domain B.

To remove much of this bias, introduced by the finite-range effect, the iterative correction approach proposed by Pickering et al. (1995) has been used. After three iterations, no further correction is predicted giving least-squares best fits to the data of $D = 1.06 \pm 0.07$, $C = 67.51 \pm 8.34$ for domain A and $D = 1.05 \pm 0.05$, $C = 67.56 \pm 5.80$ for domain B (Fig. 6c and d). However, the short length of the fitted lines, spanning one order of magnitude, makes the fractal geometry of the fault populations investigated equivocal.

To overcome this uncertainty, the box-counting technique has been used as an additional approach to the inferred power-law distributions. The procedure is to cover the fault network by a sequence of grids, then count the number of occupied boxes as a function of the box size (Hirata, 1989). A strict methodology of the box-counting analysis requires (Walsh and Watterson, 1993): a) unmapped ground outside the fault map must not be included in the area analyzed

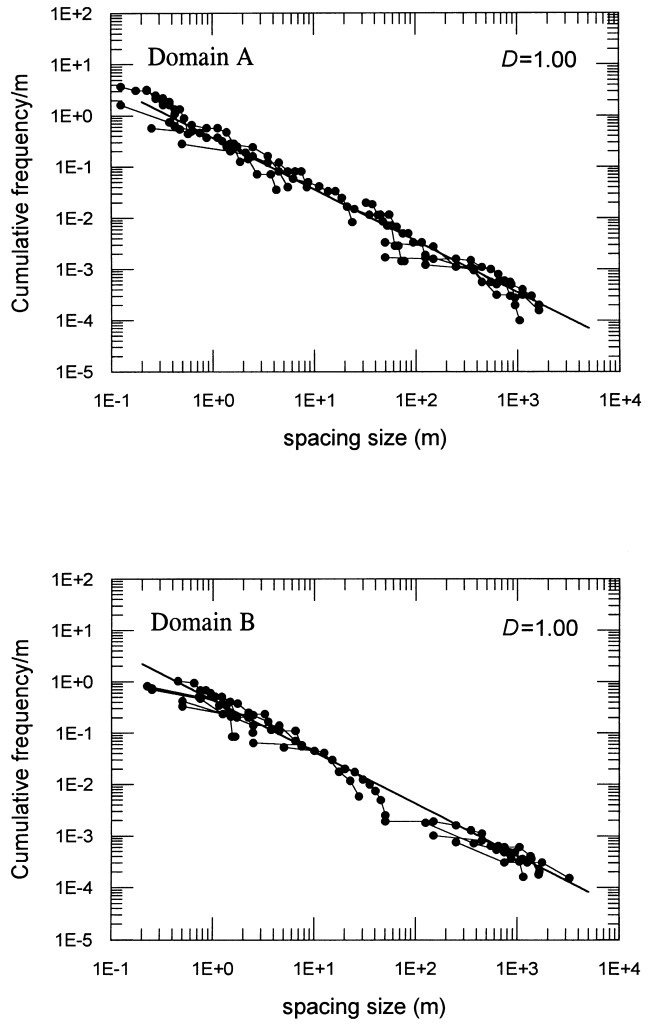

Fig. 5. Logarithmic cumulative frequency m^{-1} plots for multi-line, one-dimensional samples (lines) of fault spacing from the domains A and B.

and b) box counting should be performed over as wide a range of box sizes as is possible, but the relevant part of the curve is that corresponding to box sizes between those of the largest and smallest fault or fault spacing. To meet these criteria, which provide reliable characterization of fault patterns, the trace-length populations of the domain A and B have been analyzed using the multi-box initial grids shown in Fig. 2(b). The initial boxes are rectangles with length (parallel to the fault strike) 15 km and height 6.9 km. Given that the largest fault length is 17 km and fault lengths shorter than 1.5 km have been consistently under sampled (Fig. 6), the valid range of the box-counting curves extend to box-lengths ranging from 1.5 km to 15 km (i.e. 1–10 boxes along the abscissa) (Fig. 7a and b). Least-squares fits for these parts of the curves produce straight lines of slope −1.83 for the domain A and −1.82 for the domain B. Both lines have high correlation coefficients estimated at 0.996. Upon further examination, however, the fitted parts of the box-counting curves contain two straight segments of slopes −2 and ca −1.75 (Fig. 7c). This change in slope should not be taken as evidence of a non-fractal pattern but rather as a reflection of the inadequacies of the box-counting technique (Gillespie et al., 1993). The slopes of −2 provide an indication that all boxes with lengths ranging from 5 km to 15 km (i.e. 1–3 boxes along the abscissa) contain one or more faults (cf. Gillespie et al., 1993; Walsh and Watterson, 1993). This is interpreted in terms of a regular distribution of faults, which is consistent with the one-dimensional spacing results. The change in slope from −2 to ca −1.75 may be attributed to the left-hand truncation effect on the trace-length data. This effect, which is proportionally greater for small faults (Pickering et al., 1995), results in underestimation of the occupied boxes downscale, yielding gentler slopes of the box-counting curves for box lengths shorter than 5 km.

Further considerations of the fault trace-length data permit characterization of the fault density. The fault density is defined as the total trace length divided by the mapped area, which is estimated at 375 km^2 for the domain A and 400 km^2 for the domain B (Fig. 2b). The total fault length mapped within these areas can be estimated either by integration of Eq. (2) for the length distributions shown in Fig. 6(a and b) (Scholz and Cowie, 1990), or by a pure numerical method summing the fault lengths included in each data set (Barton and La Pointe, 1995). The results for a range of fault length truncation values are shown in Fig. 8. It is evidenced that integration of Eq. (2) produces similar fault densities for the domains A and B, which are 0.35 km/km^2 at a truncation value of 2.5 km. This fits well with the results of the numerical method. The method implies no significant variations of fault densities for truncation values greater than 2 km and yields fault densities of 0.4 km/km^2 at a resolution limit of 2.5 km. Below this limit the method predicts that domain B is less densely faulted by an amount of $\approx 100\ m/km^2$. This is most probably attributed to inadequate sampling of small faults rather than to true fault-length distributions.

Summarizing, the results of the invoked methods show that neither the fault trace-length populations, nor the involved fault densities, may adequately be differentiated between the domains A and B. Thus, it seems that fault-length distributions are independent of the amount of extension.

4.4. Fault trace and throw relationships

4.4.1. Length-maximum throw ratios

A logarithmic plot of the maximum throw (d) vs. trace-length (l) data for 45 well-constrained faults is

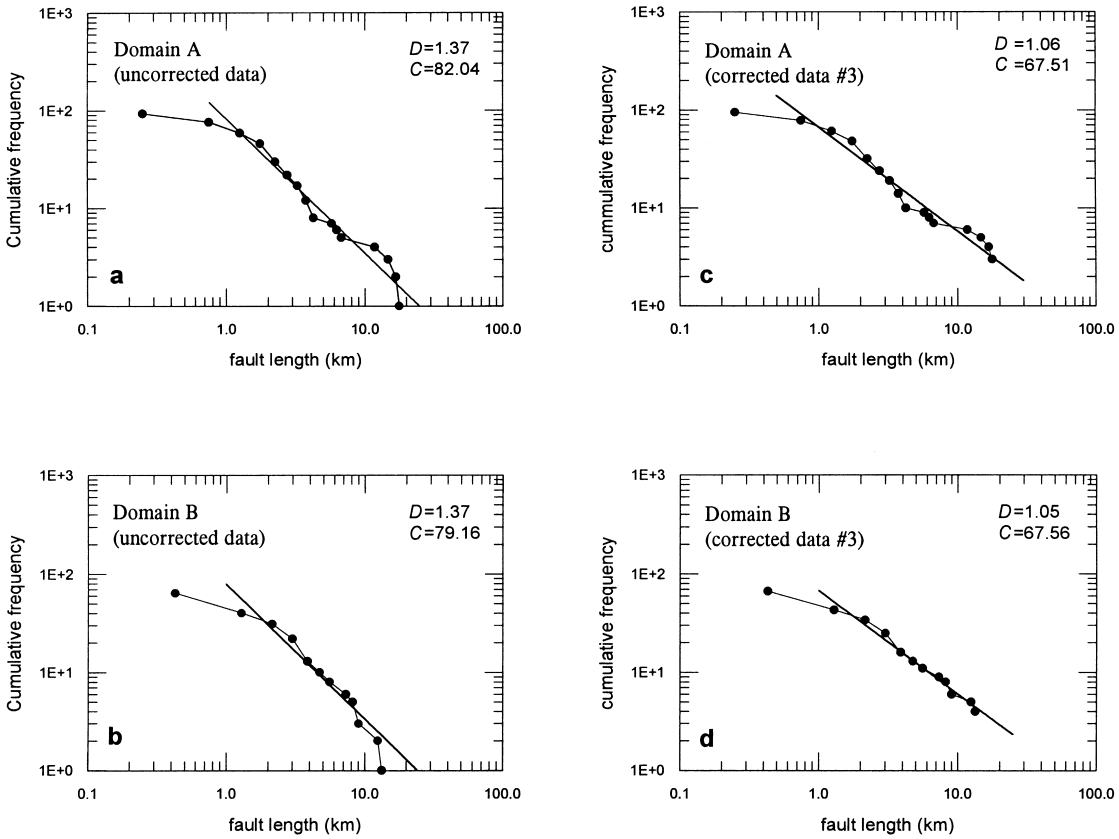

Fig. 6. Logarithmic cumulative frequency plots for fault trace-length populations of the domains A and B. (a) and (b) Plots uncorrected for the finite range effect. (c) and (d) Plots corrected for the finite range effect using the iterative correction procedure. After three iterations (#3) no further correction is predicted.

shown in Fig. 9. The data compilation and the involved errors have been discussed in a previous section of the paper. The data show a general trend towards increasing d with l, but with a large scatter of about one order of magnitude in both variables. This scatter, which is a common feature in fault studies, has long been attributed to: a) sampling effects, b) variation in material properties, c) the limitation on accumulation of displacement imposed by isostatic restoring forces, d) inaccurate data due to problems of measuring the d-values and interpreting the l-values on segmented faults, and e) growth by segment linkage (Walsh and Watterson, 1988; Cowie and Scholz, 1992b, Gillespie et al., 1992; Cartwright et al., 1995).

The size range of the data set, together with the large extent of the $d:l$ scatter, cannot justify regressing the data and only broad bands with linear trends can be deduced. The $d:l$ data define a linear band bounded by a pair of parallel straight lines with d/l ratios (γ) equal to 0.1 and 0.01. Within this broad band, the $d:l$ data for domain B are uniformly distributed, whereas those for domain A are clustered above a line with $\gamma = 0.03$. Since the parameter (γ) represents the slip-to-length ratio, it appears that the faults in the domain A have systematically larger amount of throw, up to 10 times, than those in the domain B. Assuming that the lithological variations, restricted to minor facies variations, have not influenced mechanical properties on the length scale of faults (Walsh et al., 1994), then the $d:l$ systematics ascribe a change in fault geometry through the strain space, whereby in larger strain setting incremental increases in displacement exceed incremental increases in length.

4.4.2. Length–throw profiles

Throw profiles for four well-constrained graben-forming faults (Fig. 2b, faults L1–L4) have been used to investigate the throw distribution along individual fault traces. Throws were determined for successive sections normal to the fault trace by summing the height of the fault scarp and the thickness of the sedimentary cover on the hanging wall block (Fig. 10). This calculation implicitly assumes a) not much of the sediment has been eroded away and b) synsedimentary fault motion that is evidenced by differential facies development and sediment thickness changes along the faults (Poulimenos et al., 1993). Due to the transverse fault activity, the central portions of the footwall

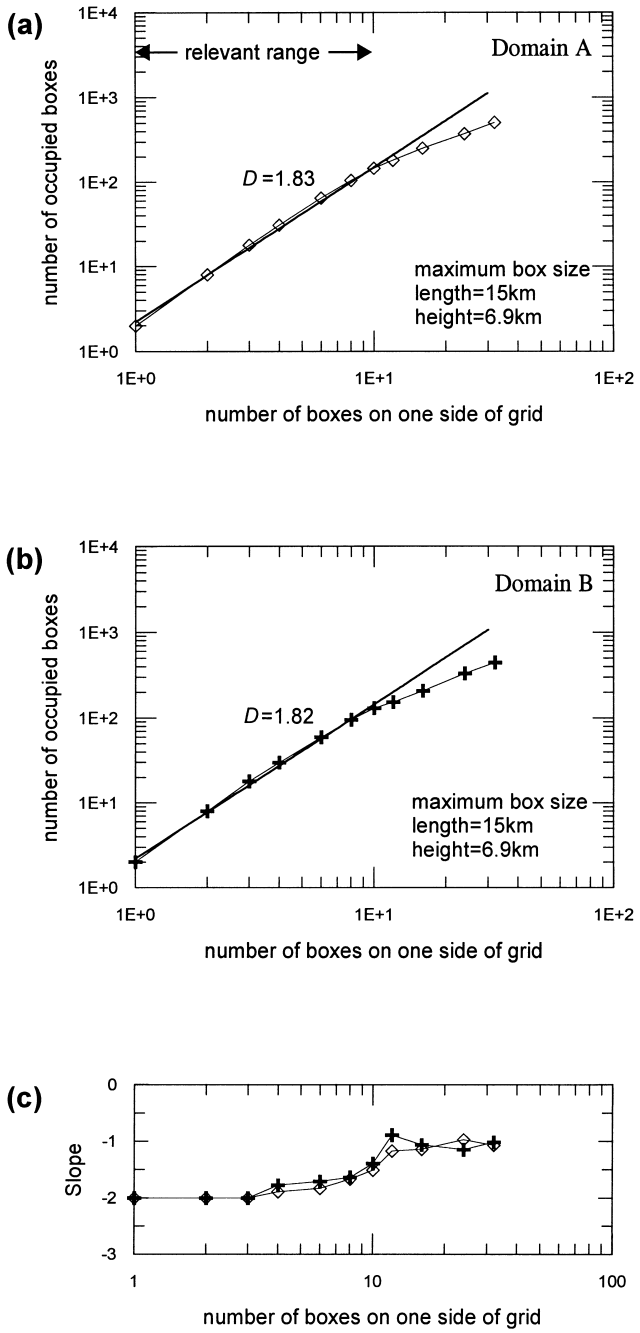

Fig. 7. (a) and (b) Box-counting curves for the domains A and B. The multi-box initial grids used for the box-counting run are shown in Fig. 2b. (c) Slopes of eleven adjacent points on curves in (a) and (b). Each slope is plotted against the number of boxes on one side of the grid.

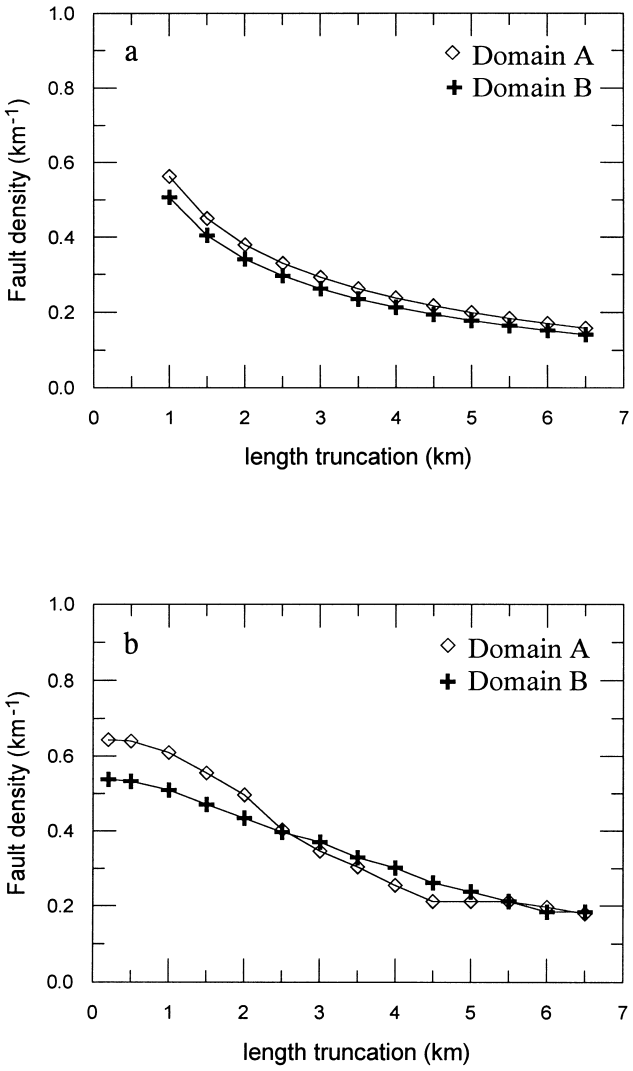

Fig. 8. Graphs showing the calculated fault densities of the domains A and B for a range of fault length truncation values. The calculations are made using: (a) Eq. (2) and (b) a purely numerical method by summing the individual fault lengths included in each of the data sets. The calculation using Eq. (2) is shown for the *D*- and *C*-values found in Fig. 6(a and b). These values determine the maximum fault length entered in calculation at $\approx$25 km for both domains. The mapped areas of the domains A and B are 375 km^2 and 400 km^2, respectively.

block topography of the faults L3 and L4 were stepped down and buried under the basin fill (Fig. 10). In these cases, the fault throws were measured by surveying the elevation difference between equivalent facies exposed at the footwall crest and the hanging wall cut-off. The exposure of the sedimentary cover, which consists of an upper coarse-grained unit and a lower fine-grained unit, is exceptionally good allowing thickness estimates to be made using maps at a scale of 1:20,000. In particular, measured thicknesses for the upper fully exposed unit ranged from 0 m to 500 m with most of the values incorporating surveying errors of less than 2%. Thickness data for the lower unit, which is fully exposed only at the base of tributary canyons, ranged from 0 m to 200 m. The maximum error associated with these measurements (i.e. surveying error plus error in total thickness) is probably no more than 10%. Fault scarp heights were resolved for

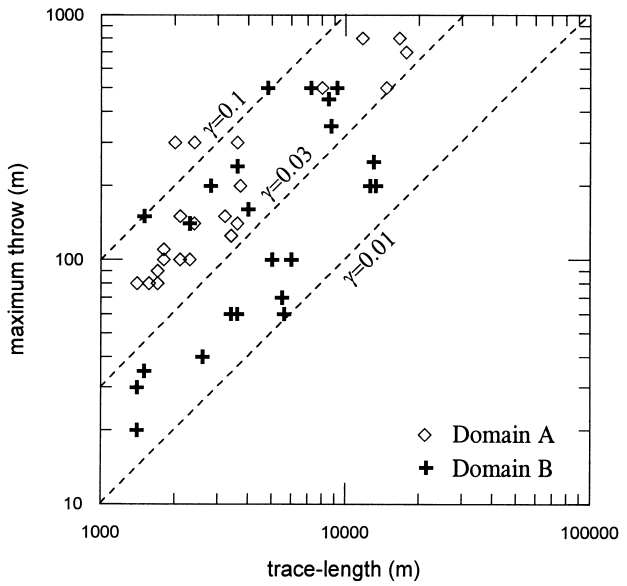

Fig. 9. Comparison of maximum throw vs. trace-length data for 45 faults surveyed in the domains A and B. The parameter γ is the ratio of maximum throw to trace-length.

calcareous scarps by using maps at a scale of 1:20,000. Scarps of up to 300 m were recorded (fig. 3B in Poulimenos et al., 1993), but values of 20–200 m were most commonly noted. Uncertainties in the scarp crest identification probably resulted in errors of about 5% for these measurements. It is therefore suggested that the profiles shown in Fig. 10 provide a useful interpretation of the fault throw distribution during the Quaternary, though the maximum values for the central parts of the faults L3 and L4 have been consistently underestimated.

The throw profiles investigated are consistent with the standard bell-shaped profiles defined by Cowie and Scholz (1992c). Both shape and throw gradients clearly demonstrate that the cumulative displacement reaches a maximum near the center of the faults and decreases gradually toward either end. Abrupt changes in throw gradient occur where the profile crosses NNE-trending faults and are likely to be due to mechanical interaction between the faults (Fig. 10). This interaction is attributed, at least in part, to elastic deformation that modifies the local shear stress acting on one fault as induced slip on the other fault (Maerten et al., 1999). Further, changes in sediment thickness and the temporal variations in depositional environments reflect a systematic migration of the fault activity during the Pleistocene time towards the central parts of the faults. High fault scarps preserved along the faults L1 and L2 are generally restricted to the central parts of the faults, which suggests that the fault slip has consistently been accumulated there. These lines of evidence indicate that near-center slip accumulation rather than lateral propagation governs the fault growth in the Corinth Graben. The proposed model does not preclude activity towards the fault ends, which is, however, too low to dominate the geomorphology and sedimentation.

5. Growth model

The observations on the strain and scaling of faults made in this study have been used to propose a geometrical model governing the evolution of the dominant, WNW-trending, normal fault set of the western Corinth graben.

The strain estimates imply that the fault population accommodates large amounts of extension, being greater in the northern part of the graben than in the southern one by as much as a factor of ≈ 1.4. However, the fault spacing populations obey similar power-law distributions for both the northern and southern rifted domains (Fig. 5). These observations, consistent with the concept of fracture saturation (Wu and Pollard, 1995; Brooks et al., 1996), suggest a deformational maturity for the Corinth graben capable of producing uniform fault spacing as the extension continues to increase. In terms of growth, the power-law spacing distributions may result from the mechanical interaction of faults (Brooks et al., 1996). If this interpretation holds, then the tip interaction could promote a growth process dominated by linkage rather than radial propagation of faults. However, it is observed that the fractal dimension D of the studied trace-length populations stays constant with increasing extension (Figs. 6 and 7). Given that, in all of the linkage models, the value of D decreases systematically with fault strain (Cartwright et al., 1995; Cladouhos and Marrett, 1996), the stabilization of the D values implies that linkage ceases to be an important process for the evolution of the fault population over the observed range of finite strains. Likewise, as the larger faults grow proportionately faster than smaller ones (Main, 1988; Cowie and Scholz, 1992b), the consistency in D values does not support a growth process dominated by fault tip propagation. In response to these constraints on fault growth, the fault trace density remains independent of strain (Fig. 8). Thus, it is shown that increasing strain correlates with increasing fault displacements and nearly constant spatial attributes of the fault population. If this is the case, then a change in fault geometry within the different strain settings must be assumed. This is clearly demonstrated by the *d:l* data sets, which demonstrate that the slip-to-length ratio systematically increases with increasing extension (Fig. 9).

Summarizing the interpretation for the fault population growth, the applied extension has progressed

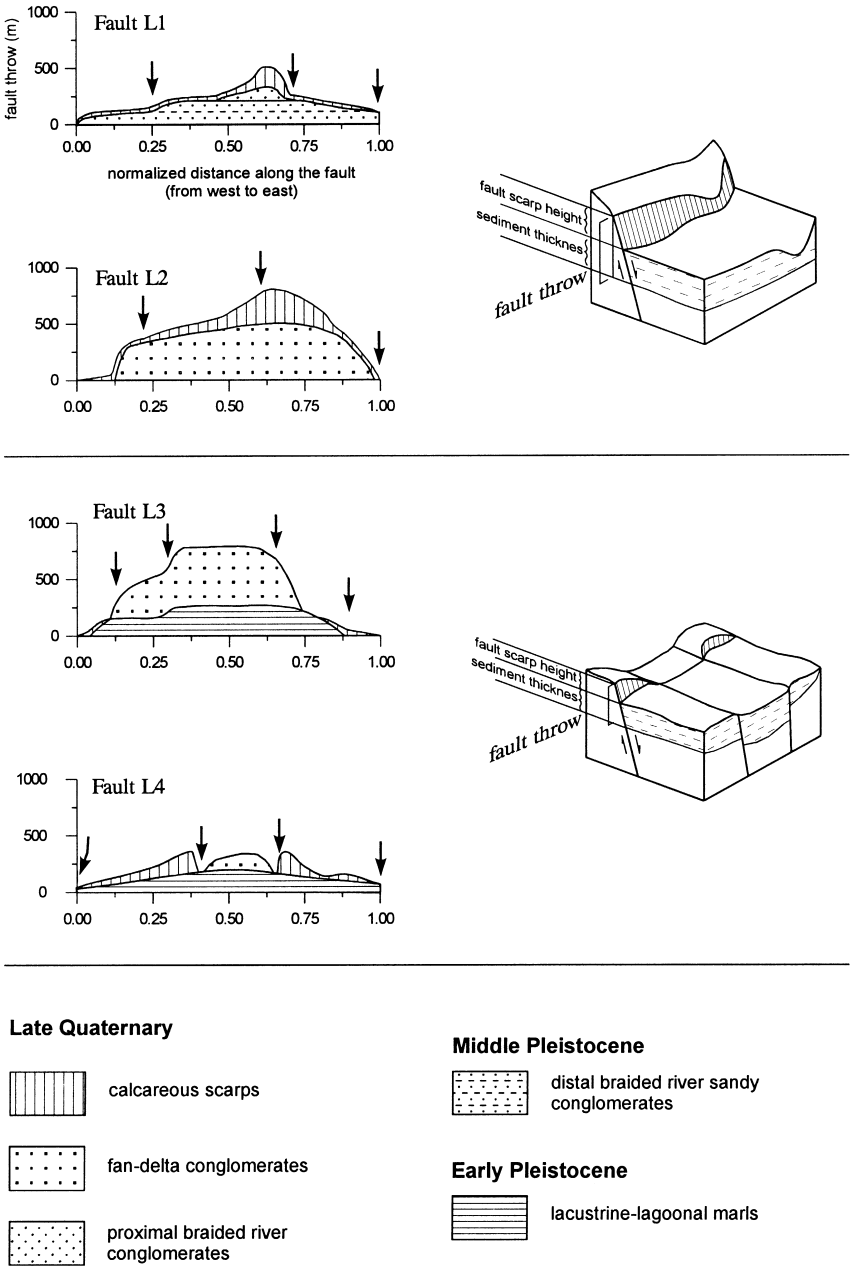

Fig. 10. Throw distributions along the WNW-trending normal faults identified in Fig. 2(b). The data have been normalized for the trace-lengths. Note the near-center location of the slip increment through time, which is controlled by the intersections with the NNE-trending faults (depicted as black arrows). The block diagrams exemplify the calculation of the fault throw.

enough to produce uniform fault spacing, and further deformation is accommodated by displacement increases rather than fault lengthening, either by segment linkage or tip propagation. The proposed model is equally applicable to single fault growth. This is evidenced by the throw profiles shown in Fig. 10, which demonstrate that near-center slip accumulation governs the fault growth during the Quaternary.

6. Discussion

The results of the fractal analysis suggest that a) the western Corinth graben has experienced large amounts of extension estimated at 30% and 22% for the northern and southern domain, respectively, and b) fault displacement increase rather fault lengthening accommodate the increasing extension.

The extension estimates were made integrating Eq. (2) from an imposed lower limit of 1 mm to the maximum observations. However, this equation tends to underestimate the extension, as the number of largest faults which accommodate most of the strain are not considered (Marrett and Allmedinger, 1991; Pickering et al., 1996). This may especially be true for the domain A where many major faults occur. Even with this deficiency the numerical results are similar to those obtained from the *d:l* relationships. Taking that the fault activity of the evolving Corinth graben migrated northwards during the Quaternary (Armijo et al., 1996; Jackson, 1999), faults in the domain B are less active and many of them older than those in the domain A. Consequently, the erosional processes lowered the scarps heights in the domain B leading to underestimation of the *d*-values and, in turn, the extension estimates and the *d:l* ratios. Whatever the accurate amount of the extension, this concept in itself supports lower finite strain for the domain B. This is also mirrored in the depositional environments of the sedimentary fill. Lacustrine/marine and terrestrial sediments have accumulated in the domains A and B, respectively (Doutsos et al., 1988), suggesting that the fault throws in the domain A were efficient in keeping the hanging wall blocks below the Pleistocene sea level, whereas those in the domain B were not. There is thus ample evidence to support differing amounts of extension, being greater in the northern part of the graben than the southern one.

The most attractive mechanical interpretation for the proposed deformation pattern involves a stress feedback mechanism operating in the seismogenic upper crust. This mechanism proposed by Cowie (1998) is based on the idea that the seismic rupture of a fault perturbs the surrounding stress field. In the case of normal fault rupture, regions of stress increase, that is positive stress change, lie along strike from the zone, while regions where the stress level is reduced, that is negative stress change, extend transverse to the rupture fault. As a consequence, even within uniform tectonic straining, some faults develop higher displacement rates and grow more rapidly while others experience reduced rates or become inactive. In this context, negative feedback resulting from fault activity in the northern domain of the Corinth graben provides a powerful explanation for the low amount of extension observed in the southern domain.

A question now arises: why do faults continue to accumulate displacement without any further lateral growth? Two possible explanations exist. The first explanation invokes the stress feedback mechanism. At a mature stage of fault development, this mechanism predicts complete linkage of existing fault segments which develop enhanced displacement rates on their central portions, whereas the tip regions change very little (Cowie, 1998). As deformation progresses, however, this pattern of linkage and enhanced growth rates may be repeated at larger scales as larger structures interact. The second explanation involves fault interaction that impedes lateral propagation. Indeed, the principal WNW-trending normal faults have propagated all along the entire rift zone, but they often abut or intersect the NNE-trending transverse faults (Fig. 2a). Hence, much or all of a normal slip distribution along the WNW-trending faults could be stopped or laterally shifted along the transverse faults (Fig. 10). Such transverse faults are characteristic of all extensional terranes (Gibbs, 1984; Larsen, 1988; Destro, 1995) and can act as either conservative or non-conservative barriers to faulting (Bruhn et al., 1987; Roberts, 1996b; Morewood and Roberts, 1997). They transfer or display displacements along extension faults and both dip-slip and oblique sense of movement are possible depending on the relative orientation of the adjacent normal fault segments.

Although the offered model for fault growth in the western Corinth graben conflicts with the widespread acceptance of faults growing by nearly proportional increase in displacement and length, it is comparable with results derived from other published data in the eastern Gulf of Corinth and regions of active extension worldwide. Geological and morphological observations supported by mechanical model suggest a marginal fault of constant length increasing steadily in displacement for the eastern Gulf of Corinth (Armijo et al., 1996). Observations of deformed marine terraces and drainage in the eastern end of the Gulf of Corinth show that the length of a major active fault has remained fixed, implying progressive increase in the values for the displacement–length ratio (Morewood and Roberts, 1999). Furthermore, Walsh and Watterson (1987) and Gillespie et al. (1992) predict an increase in the slip-to-length ratio as successive slip events accumulate on the fault. Cartwright et al. (1995) state that the final stage in the growth cycle is marked by accumulation of displacement on the linked faults with no or little fault lengthening. Willemse et al. (1996) find that slip-to-length ratio increases with increasing fault displacement. Wojtal (1994) and Filbrandt et al. (1994), show that variations in slip-to-length ratio of more than one order of magnitude should be expected during the temporal evolution of faults, even for the simplest case of a slip event in a homogeneous isotropic rock, because: (1) faults are not infinite in extent but are bounded in three dimensions; and (2) because neighboring faults or fault segments can interact.

7. Conclusions

The findings of this study can be summarized as follows:

1. In the western Corinth graben, the dominant population of WNW-trending normal faults are oriented approximately perpendicular to the opening direction and are characterized by power-law scaling properties.
2. Multi-line one-dimensional data sets of fault throw per unit distance, obtained from both the northern and the younger southern rifted domains of the graben, yield scaling power-laws of $D \approx 0.9$. Numerical evaluation of the throw populations allows the applied extension to be estimated at 30% and 22% for the northern and southern domains, respectively.
3. Fault spacing distributions for both the rifted domains derived from multi-line one-dimensional data sets, follow power-law scaling relationships with $D \approx 1$ suggestive of a regular distribution of faults within and between the domains. This uniform spacing distribution, which is not influenced by the applied large strains, is interpreted to represent a fracture saturation state.
4. Fault trace-length data, analyzed by the cumulative frequency and the box-counting techniques, obey the same power-law relationships for both the rifted domains. The cumulative frequency distributions corrected for the finite-range effect give $D \approx 1$, compared to the biased D-values of ≈ 1.4, whereas the box-counting curves yield $D \approx 1.8$. The fault densities, estimated from the cumulative frequency distributions, are 0.4 km/km^2 at a fault length truncation value of 2.5 km for both domains. This overall consistency suggests that the trace-length distribution is independent of strain.
5. Plots of maximum throw (d) vs. trace-length (l) show a band distribution bounded by a pair of parallel lines with $d/l \approx 0.1$ and 0.01. Within this band, the d/l for the northern domain is systematically higher than for the southern domain, suggesting that as extension increases slip accumulation dominates the fault growth. This growth process is consistent with field observations on fault throw distribution along individual graben forming faults.

The observations on the strains and the scaling properties are used to suggest that the applied strain has reached a certain value capable of producing constant spacing distributions for the normal fault population, which evolves with accumulation of fault displacement rather than fault lengthening. Possible explanations for this deformation pattern include: 1) a stress feedback mechanism which allows enhanced displacement rates on those faults that are optimally positioned in the overall fault population and 2) the mechanical interaction between the WNW-trending normal faults with a set of NNE-trending transverse faults that impede lateral propagation.

Acknowledgements

I am grateful to Patience Cowie, David Sanderson and Jonathon Imber for thorough reviews and insightful suggestions on earlier versions of this manuscript. The paper was substantially improved by reviews from G. Roberts and T. Needham.

References

Ambraseys, N., Jackson, J., 1990. Seismicity and strain in central Greece between 1890 and 1988. Geophysical Journal International 101, 663–708.

Armijo, R., Meyer, B., King, G.C.P., Rigo, A., Papanastassiou, D., 1996. Quaternary evolution of the Corinth Rift and its implications for the Late Cenozoic evolution of the Aegean. Geophysical Journal International 126, 11–53.

Barton, C.C., La Pointe, P.R., 1995. Fractals in the Earth Sciences. Plenum Press, New York.

Boggs Jr., S., 1987. Principles of Sedimentology and Stratigraphy. Merrill Publishing Company, Ohio.

Brooks, B.A., Almendinger, R.W., de la Barra, I.G., 1996. Fault spacing in the El Teniente Mine, central Chile: Evidence for nonfractal fault geometry. Journal of Geophysical Research 10, 13633–13653.

Brooks, M., Ferentinos, G., 1984. Tectonics and sedimentation in the Gulf of Corinth and the Zakynthos and Kefallinia channels, western Greece. Tectonophysics 101, 25–54.

Bruhn, R., Gibler, P.R., Parry, W.T., 1987. Rupture characteristics of normal faults: an example from the Wasatch fault zone, Utah. In: Coward, M.P., Dewey, J.F., Hancock, P.L. (Eds.), Continental Extensional Tectonics, Geological Society of London Special Publication 28, pp. 337–353.

Brunet, M.A., Le Pichon, X., 1982. Subsidence of the Paris Basin. Journal of Geophysical Research 87, 8547–8560.

Cartwright, J.A., Trudgill, B.D., Mansfield, C.S., 1995. Fault growth by segment linkage: an explanation for scatter in maximum displacement and trace length data from the Canyonlands Grabens of SE Utah. Journal of Structural Geology 17, 1319–1326.

Cladouhos, T.T., Marrett, R., 1996. Are fault growth and linkage models consistent with power-law distributions of fault lengths? . Journal of Structural Geology 18, 281–293.

Colletta, B., Le Quellec, P., Letouzey, J., Moretti, I., 1988. Longitudinal evolution of the Suez rift structure (Egypt). Tectonophysics 153, 221–233.

Cowie, P.A., Scholz, C.H., 1992a. Growth of faults by accumulation of seismic slip. Journal of Geophysical Research 10, 11085–11095.

Cowie, P.A., Scholz, C.H., 1992b. Displacement–length relationship for faults: data synthesis and discussion. Journal of Structural Geology 14, 1149–1156.

Cowie, P.A., Scholz, C.H., 1992c. Physical explanation for the displacement–length relationship of faults, using a post-yield fracture mechanics model. Journal of Structural Geology 14, 1133–1148.

Cowie, P.A., 1998. A healing–reloading feedback control on the growth rate of seismogenic faults. Journal of Structural Geology 20, 1075–1089.

Destro, N., 1995. Release fault: A variety of cross fault in linked extensional fault systems, in the Sergipe–Alagoas Basin, NE Brazil. Journal of Structural Geology 17, 615–629.

Doutsos, T., Kontopoulos, N., Poulimenos, G., 1988. The Corinth–Patras rift as the initial stage of continental fragmentation behind an active island arc (Greece). Basin Research 1, 177–190.

Doutsos, T., Piper, D.J.W., 1990. Listric faulting, sedimentation and morphological evolution of the Quaternary eastern Corinth graben: first stages of continental rifting. Geological Society of America Bulletin 102, 812–829.

Doutsos, T., Poulimenos, G., 1992. Geometry and kinematics of active faults and their seismotectonic significance in the western Corinth–Patras rift (Greece). Journal of Structural Geology 14, 686–699.

Ellis, M.A., Dunlap, W.J., 1988. Displacement variation along thrust faults: implications for the development of large faults. Journal of Structural Geology 10, 183–192.

Filbrandt, J.M., Richard, P.D., Franssen, R.C.M.W., 1994. Growth and coalescence of faults: numerical simulations and sand-box experiments. In: TSG Special Meeting on Fault Populations, Edinburgh, U.K., Extended Abstracts, pp. 57–59.

Gibbs, A.D., 1984. Structural evolution of extensional basin margins. Journal of Structural Geology 141, 609–620.

Gillespie, P.A., Walsh, J.J., Watterson, J., 1992. Limitations of dimension and displacement data from single faults and the consequences for data analysis and interpretation. Journal of Structural Geology 14, 1157–1172.

Gillespie, P.A., Howard, C.B., Walsh, J.J., Watterson, J., 1993. Measurement and characterisation of spatial distributions of fractures. Tectonophysics 226, 113–141.

Harris, C., Franssen, R., Loosveld, R., 1991. Fractal analysis of fractures in rocks: the Cantor's Dust method—comment. Tectonophysics 198, 107–115.

Heffer, K.J., Bevan, T. 1990. Scaling relationships in natural fractures—Data, theory and applications. Society of Petroleum Engineers Reprint No. 20981, pp. 1–12.

Hirata, T., 1989. Fractal dimension of fault systems in Japan: Fractal structure in rock fracture geometry at various scales. Pure and Applied Geophysics 131, 157–169.

Jackson, J., 1999. Fault death: a perspective from actively deforming regions. Journal of Structural Geology 21, 1003–1010.

Jackson, J., McKenzie, D., 1988. Rates of active deformation in the Aegean Sea and surrounding regions. Basin Research 1, 121–128.

Jackson, P., Sanderson, D.J., 1992. Scaling of fault displacements from the Badajoz–Cordoba shear zone, SW Spain. Tectonophysics 210, 179–190.

Jolivet, L., Brun, J.P., Gautier, P., Lallemant, S., Patriat, M., 1994. 3-D kinematics of extension in the Aegean region from the early Miocene to the Present, insights from the ductile crust. Bulletin de la Societe Geologique de France 165, 195–209.

Larsen, P.H., 1988. Relay structures in a Lower Permian basement-involved extension system. East Greenland. Journal of Structural Geology 10, 3–8.

Le Pichon, X., Angelier, J., 1981. The Aegean Sea. Philosophical Transactions of the Royal Society of London A300, 357–372.

Maerten, L., Emanuel, E.J.M., Pollard, D.D., Rawnsley, K., 1999. Slip distributions on intersecting normal faults. Journal of Structural Geology 21, 259–271.

Main, I.G., 1988. Prediction of failure times in the earth for a time varying stress. Geophysical Journal 92, 455–464.

Mandelbrot, B.B., 1983. The Fractal Geometry of Nature. Freeman Press, New York.

McKenzie, D., 1978. Active tectonics of the Alpine–Himalayan belt: the Aegean Sea and surrounding regions. Geophysical Journal of the Royal Astronomical Journal 55, 217–254.

Marrett, R.A., Allmedinger, R.W., 1991. Estimates of strain due to brittle faulting: sampling of fault populations, Kinematic analysis of fault-slip data. Journal of Structural Geology 13, 735–738.

Martel, S.J., Pollard, D.D., Segall, P., 1988. Development of simple strike-slip fault zones, Mount Abbot quadrangle, Sierra Nevada, California. Geological Society of America Bulletin 100, 1451–1465.

Morewood, N.C., Roberts, G.P., 1997. The geometry, kinematics and rates of deformation in a normal fault segment boundary, central Greece. Geophysical Research Letters 24, 3081–3084.

Morewood, N.C., Roberts, G.P., 1999. Lateral propagation of the surface trace of the South Alkyonides normal fault segment, central Greece: its impact on models of fault growth and displacement–length relationships. Journal of Structural Geology 21, 635–652.

Narr, W., 1991. Fracture density in the deep subsurface: Techniques with application to Point Arguello oil field. American Association of Petroleum Geologists Bulletin 75, 1300–1323.

Needham, T., Yielding, G., Fox, R., 1996. Fault population description and prediction using examples from the offshore U.K. Journal of Structural Geology 18, 155–167.

Peacock, D.C.P., Sanderson, D.J., 1991. Displacements, segment linkage and relay ramps in normal fault zones. Journal of Structural Geology 13, 721–733.

Peacock, D.C.P., Sanderson, D.J., 1994. Strain and scaling of faults in the chalk at Flamborough Head, U.K. Journal of Structural Geology 16, 97–107.

Pickering, G., Bull, J.M., Sanderson, D.J., 1995. Sampling power-law distributions. Tectonophysics 248, 1–20.

Pickering, G., Bull, J.M., Sanderson, D.J., 1996. Modern Developments in Structural Interpretation, Validation and Modelling. In: Buchanan, P.G., Nieuwland, D.A. (Eds.), Geological Society of London Special Publication 99, pp. 11–26.

Poulimenos, G., 1993. Tectonics and sedimentation in the western Corinth graben. Neues Jahrbuch fur Geologie und Palaontologie Monatshefte 10, 607–630.

Poulimenos, G., Doutsos, T., 1997. Flexural uplift of rift flanks in central Greece. Tectonics 16, 912–923.

Poulimenos, G., Albers, G., Doutsos, T., 1989. Neotectonic evolution of the central section of the Corinth graben. Zeitschrift der deutschen geologischen Gesellschaft 140, 173–182.

Poulimenos, G., Zelilidis, A., Kontopoulos, N., Doutsos, T., 1993. Geometry of trapezoidal fan deltas and their relationship to extensional faulting along the south-western active margins of the Corinth rift, Greece. Basin Research 5, 179–192.

Richard, H., Groshong, J.R., 1996. Construction and validation of extensional cross-sections using lost area and strain, with application to the Rhine Graben. In: Buchanan, P.G., Nieuwland, D.A. (Eds.), Construction and validation of extensional cross-sections using lost area and strain, with application to the Modern Developments in Structural Interpretation, Validation and Modelling, Geological Society of London Special Publication 99, pp. 79–87.

Rigo, A., Lyon-Caen, H., Armijo, R., Deschamps, A., Hatzfeld, D., Makropoulos, K., Papadimitriou, P., Kassaras, I., 1996. A microseismic study in the western part of the Gulf of Corinth (Greece): implications for large-scale normal faulting mechanisms. Geophysical Journal International 126, 663–688.

Roberts, G.P., 1996a. Variation in fault-slip directions along active and segmented normal fault systems. Journal of Structural Geology 18, 835–845.

Roberts, G.P., 1996b. Noncharacteristic normal faulting surface ruptures from the Gulf of Corinth, Greece. Journal of Geophysical Research 101, 25255–25267.

Roberts, S., Jackson, J., 1991. Active normal faulting in central Greece: an overview. In: Roberts, A.M., Yielding, G., Freeman, B. (Eds.), The geometry of Normal Faults, Geological Society of London Special Publication 56, pp. 125–142.

Scholz, C.H., Aviles, C., 1986. Earthquake Source Mechanisms. In: Das, S., Boatwright, J., Scholz, C. (Eds.), Geophysical Monograph Series 37, pp. 147–155.

Scholz, C.H., Cowie, P.A., 1990. Determination of total strain from faulting using slip measurements. Nature 346, 837–839.

Segall, P., Pollard, D.D., 1980. Mechanics of discontinuous faults. Journal of Geophysical Research 85, 4337–4350.

Sornette, A., Davy, Ph., Sornette, D., 1990. Growth of fractal fault patterns. Physical Review Letters 65, 2266–2269.

Turcotte, D.L., 1989. Fractals in geology and geophysics. Pure and Applied Geophysics 131, 171–196.

Walsh, J.J., Watterson, J., 1987. Distributions of cumulative displacement and seismic slip on a single normal fault surface. Journal of Structural Geology 9, 1039–1046.

Walsh, J.J., Watterson, J., 1988. Analysis of the relationship between displacement and dimensions of faults. Journal of Structural Geology 10, 239–247.

Walsh, J.J., Watterson, J., Yielding, G., 1991. The importance of small-scale faulting in regional extension. Nature 351, 391–393.

Walsh, J.J., Watterson, J., 1992. Populations of fault displacements and their effects on estimates of fault-related regional extension. Journal of Structural Geology 14, 701–712.

Walsh, J.J., Watterson, J., 1993. Fractal analysis of fracture patterns using the standard box-counting technique: valid and invalid methodologies. Journal of Structural Geology 15, 1509–1512.

Walsh, J.J., Watterson, J., Yielding, G., 1994. Determination and Interpretation of Fault size Populations: Procedures and Problems. North Sea Oil and Gas Reservoirs III, 141–155.

Watterson, J., 1986. Fault dimensions, displacements and growth. Pure and Applied Geophysics 124, 365–373.

Westaway, R., 1994. Quantitative analysis of populations of small faults. Journal of Structural Geology 16, 1259–1273.

Willemse, E.J.M., Pollard, D.D., Aydin, A., 1996. Three-dimensional analysis of slip distributions on normal fault arrays with consequences for fault scaling. Journal of Structural Geology 18, 295–309.

Wojtal, S.F., 1994. Fault scaling laws and temporal evolution of fault systems. Journal of Structural Geology 16, 603–612.

Wu, H., Pollard, D.D., 1992. Propagation of a set of opening-mode fractures in layered brittle materials under uniaxial strain cycling. Journal of Geophysical Research 97, 3381–3396.

Wu, H., Pollard, D.D., 1995. An experimental study of the relationship between joint spacing and layer thickness. Journal of Structural Geology 17, 887–905.

Yielding, G., Walsh, J.J., Watterson, J., 1992. The prediction of small-scale faulting in reservoirs. First Break 10, 449–460.